nature astronomy

Article

https://doi.org/10.1038/s41550-024-02267-y

Low-temperature formation of pyridine and (iso)quinoline via neutral–neutral reactions

Received: 21 February 2023

Accepted: 9 April 2024

Published online: 13 May 2024

Check for updates

Zhenghai Yang[1], Chao He[1], Shane J. Goettl[1], Alexander M. Mebel[2] ✉, Paulo F. G. Velloso[3], Márcio O. Alves[3], Breno R. L. Galvão[3] ✉, Jean-Christophe Loison[4] ✉, Kevin M. Hickson[4], Michel Dobrijevic[5], Xiaohu Li[6,7] ✉ & Ralf I. Kaiser[1] ✉

Aromatic molecules represent fundamental building blocks in prebiotic chemistry and are contemplated as vital precursors to DNA and RNA nitrogen bases. However, despite the identification of some 300 molecules in extraterrestrial environments, the pathways to pyridine (C_5H_5N), pyridinyl ($C_5H_4N\cdot$) and (iso)quinoline (C_9H_7N)—the simplest representative mono- and bicyclic aromatic molecules carrying nitrogen—are elusive. Here we afford compelling evidence on the gas-phase formation of methylene amidogen ($H_2CN\cdot$) and cyanomethyl ($H_2CCN\cdot$) radicals via molecular beam studies and electronic structure calculations. The modelling of the chemistries of the Taurus molecular cloud (TMC-1) and Titan's atmosphere contemplates a complex chain of reactions synthesizing pyridine, pyridinyl and (iso) quinoline from $H_2CN\cdot$ and $H_2CCN\cdot$ at levels of up to 75%. This study affords unique entry points to precursors of DNA and RNA nitrogen bases in hydrocarbon-rich extraterrestrial environments thus changing the way we think about the origin of prebiotic molecules in our Galaxy.

Since the first discovery of biorelevant, heteroaromatic molecules such as vitamin B3 (niacin)[1,2] and nucleobases (pyrimidines, purines)[3] in carbonaceous chondrites, including Murchison[3,4], critical questions have arisen on their formation routes in extraterrestrial environments. The identification of a series of terrestrially rare nucleobases such as 6-diaminopurine along with $^{15}N/^{14}N$ isotope enrichment suggests an interstellar origin[4], thus providing a vital link between cold molecular clouds as their origin and their identification in our Solar System. Their stem compounds—polycyclic aromatic hydrocarbons (PAHs) along with their cations and (partially) hydrogenated counterparts[5–7]—have been proposed to be associated with the synthesis of these biorelevant molecules in the interstellar medium, although it has not been unravelled how a stable C–H moiety in PAHs can be replaced by an isoelectronic nitrogen atom (N) in NPAHs. The 6.2 μm (1,613 cm^{-1}) infrared emission band in deep space has been linked to protonated PAHs[8], but has also been discussed as the result of NPAHs[9], with PAHs and NPAHs accounting for up to 30% of the cosmic carbon budget[10]. Whereas well-defined low-temperature (cold molecular clouds; Taurus molecular cloud (TMC-1)) and high-temperature (circumstellar envelopes; IRC+10216) routes to PAH formation have begun to emerge[11], surprisingly little is known on the gas-phase synthesis of their nitrogen-substituted counterparts (NPAHs). This lack of knowledge is rather staggering considering that these aromatics carry the cyclic nitrogen–carbon skeletons of a key class of astrobiologically important molecules: nitrogen bases of deoxyribonucleic acid (DNA) and ribonucleic acid (RNA)[9,12].

Recent astrochemical models indicate that the carbon–nitrogen chemistries in molecular clouds can be linked with complex reaction networks[13] of gas-phase ion–molecule[14] and neutral–neutral reactions[15] of aromatic and resonantly stabilized free radicals such as phenyl ($C_6H_5\cdot$) and propargyl ($C_3H_3\cdot$), along with their nitrogen counterparts

[1]Department of Chemistry, University of Hawaii at Manoa, Honolulu, HI, USA. [2]Department of Chemistry and Biochemistry, Florida International University, Miami, FL, USA. [3]Centro Federal de Educação Tecnológica de Minas Gerais, CEFET-MG, Belo Horizonte, Brazil. [4]Institut des Sciences Moléculaires, CNRS, Université de Bordeaux, Talence, France. [5]Laboratoire d'Astrophysique de Bordeaux, Université de Bordeaux, CNRS, Pessac, France. [6]Xinjiang Astronomical Observatory, Chinese Academy of Sciences, Urumqi, P. R. China. [7]Key Laboratory of Radio Astronomy, Chinese Academy of Sciences, Urumqi, P. R. China. ✉e-mail: mebela@fiu.edu; brenogalvao@gmail.com; jean-christophe.loison@cnrs.fr; xiaohu.li@xao.ac.cn; ralfk@hawaii.edu

https://doi.org/10.1038/s41550-024-02267-y

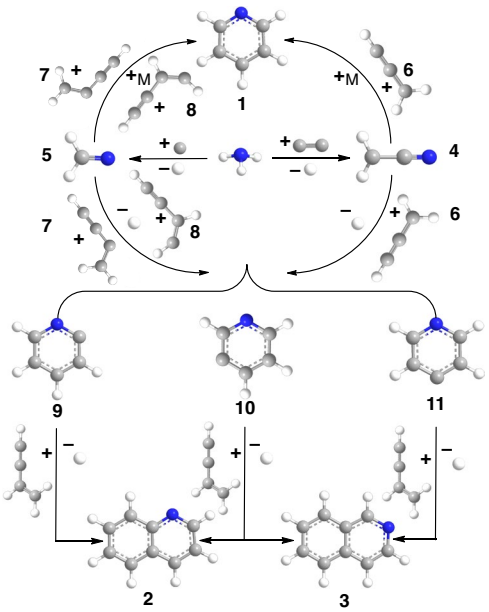

Fig. 1 | Pathways to pyridine and (iso)quinoline. A chain of reactions initiated through the formation of methylene amidogen ($H_2CN\cdot$, **5**) and cyanomethyl ($H_2CCN\cdot$, **4**) lead to the simplest representatives of mono- and bicyclic aromatic molecules carrying nitrogen. The reactions of atomic carbon and dicarbon with ammonia to $H_2CN\cdot$ and $H_2CCN\cdot$ are investigated via a crossed molecular beam machine; our calculations predict the formation of pyridine (**1**) and pyridinyl radicals (**9**–**11**) through the reactions of $H_2CN\cdot$ with *i*/*n*-C_4H_3 and of $H_2CCN\cdot$ with propargyl (C_3H_3). In Titan's atmosphere, pyridine can be stabilized by a third body with a bath molecule such as molecular nitrogen (M = N_2). The reactions of pyridinyl radicals (**9**–**11**) with vinylacetylene (C_4H_4) forming (iso)quinoline are depicted in ref. 29.

pyridinyl ($C_5H_4N\cdot$) and cyanomethyl ($H_2CCN\cdot$)[14,16–18]. Furthermore, the synthesis of pyridine (C_5H_5N) has been proposed to be driven by radical-mediated reactions of hydrogen cyanide (HCN)[19] and via de facto methylidyne radical (CH) insertion into pyrrole (C_4H_5N)[20]. These reaction networks have been 'borrowed' from the planetary science community attempting to rationalize the existence of both stratospheric PAHs and NPAHs in Titan's atmosphere determined from Cassini's Visual and Infrared Mapping Spectrometer (VIMS) measurements at 3.28 μm (3,049 cm^{-1})[21] and Composite Infrared Spectrometer (CIRS) measurements at 71.43 μm (140 cm^{-1})[22,23], and through Cassini's Plasma Spectrometer (CAPS)[24]. The latter detected positively and negatively charged particles with molecular weights of less than 8,000 AMU containing (N)PAHs along with their fundamental building blocks benzene (C_6H_6; m/z = 78) and pyridine (C_5H_5N; m/z = 79)[14,24,25]. Overall, so far, an understanding of the synthesis of benzene along with aromatics carrying up to six rings such as corannulene ($C_{20}H_{10}$)[26] and helicenes ($C_{26}H_{16}$)[27] is beginning to emerge[11]. However, the underlying elementary processes leading to the simplest representatives of mono- and bicyclic aromatic molecules carrying nitrogen, that is, pyridine (C_5H_5N; **1**) and (iso)quinoline (C_9H_7N; **2**/**3**), together with their cyanomethyl ($H_2CCN\cdot$; **4**) and methylene amidogen ($H_2CN\cdot$; **5**) precursors, is still in its infancy (Fig. 1). The understanding of these gas-phase reactions and the formation of the first carbon–nitrogen bonds from the 'bottom up' is fundamental to our knowledge of how nitrogen-containing aromatics can be produced abiotically in low-temperature interstellar and Solar System environments from the simple closed-shell nitrogen-containing hydride (ammonia; NH_3) and reactive carbon-based reactants in form of atomic carbon (C) and dicarbon (C_2).

Here we report on the gas-phase preparation of the methylene amidogen radical ($H_2CN\cdot$, X^2B_2) and of the resonantly stabilized cyanomethyl radical ($H_2CCN\cdot$, X^2B_1) via bimolecular reactions of atomic carbon (C, ^3P) and of dicarbon (C_2, $X^1\Sigma_g^+/a^3\Pi_u$) with ammonia (NH_3, X^1A_1), exploiting crossed molecular beam experiments. Combined with electronic structure calculations and modelling of the chemistries of hydrocarbon-rich environments of cold molecular clouds and atmospheres of planets and their moons exploiting TMC-1 (10 K) and Titan (70–180 K) as benchmarks, the role of the methylene amidogen and the cyanomethyl radicals in forming pyridine (C_5H_5N; **1**), pyridinyl (C_5H_4N; **9**–**11**) and (iso)quinoline (C_9H_7N; **2**/**3**) is also elucidated. In addition, a complex chain of exoergic, barrierless routes is contemplated with $H_2CN\cdot$ and $H_2CCN\cdot$ radicals representing fundamental molecular building blocks of pyridine and pyridinyl radicals ($C_5H_4N\cdot$, **9**–**11**) synthesized through successive barrierless reactions involving propargyl ($C_3H_3\cdot$, X^2B_1, **6**) and *i*/*n*-$C_4H_3\cdot$ (X^2A', **7** and **8**) under low-temperature conditions[28] (Fig. 1). As pyridinyl radicals are isoelectronic to the phenyl radical ($C_6H_5\cdot$), pyridinyl may play a critical role in the gas-phase formation of (iso)quinoline upon reaction with vinylacetylene (C_4H_4) via the low-temperature hydrogen abstraction–vinylacetylene addition pathway[29]. These results thus offer fundamental knowledge on the previously elusive reaction routes to prototype nitrogen heteroaromatics not only in TMC-1 and Titan's atmosphere but also in low-temperature, hydrocarbon- and nitrogen-rich atmospheres of outer Solar System bodies such as Triton[30] and Pluto[31]. Hence, the present work sheds light on sensible processes coupling the carbon and nitrogen chemistries eventually leading to the formation of molecular nitrogen–carbon motives of astrobiological relevance as found in, for example, nucleobases[29] in our Universe.

Results

Laboratory frame

The reactive scattering signal of the reaction of atomic carbon (C, ^3P) with D3-ammonia (ND_3, X^1A_1) was observed at m/z = 30 (D_2CN^+); where D is deuterium. Within our signal to noise, no signal was monitored at 32 (D_3CN^+), indicating that no D_3CN adducts were formed. These data alone indicate the existence of the D-loss channel (reaction (1)). Note that for technical reasons, the reaction was not conducted with ammonia (NH_3, X^1A_1) as this would have shifted the reactive scattering signal to m/z = 28 (H_2CN^+). The signal at 28 is obscured by substantial background counts from carbon monoxide, which outgasses from stainless steel even under our ultrahigh-vacuum conditions of 6×10^{-12} torr. Therefore, angle-resolved time-of-flight (TOF) spectra were recorded at 30 (D_2CN^+) in 5° intervals within the scattering plane, integrated and scaled with respect to the TOF recorded at the centre-of-mass (CM) angle of 35.9 ± 0.5° leading to the laboratory angular distribution (LAD). This distribution holds a maximum around the CM angle and is nearly forward–backward symmetric (Fig. 2a,b), implying that the carbon–D3-ammonia reaction proceeds through indirect reaction dynamics involving the formation of D_3CN collision complex(es).

The reactive scattering signal of the reaction of dicarbon (C_2, $X^1\Sigma_g^+/a^3\Pi_u$) with ammonia (NH_3, X^1A_1) was detected at m/z = 40 ($C_2NH_2^+$) and 39 (C_2NH^+) (reaction (2)) with the signal at 39 collected at the level of 66 ± 5% compared with the signal at 40. The TOF spectra at 40 and 39 are identical after scaling, suggesting that the signal at 39 originates from dissociative ionization of the nascent product (40 AMU). Furthermore, the signal at 40 indicated the existence of H loss and inherent formation of a molecule with the molecular formula C_2NH_2. Consequently, data were collected at 40 in 2.5° steps (Fig. 2c,d). The derived LAD is also nearly forward–backward symmetric, revealing the existence of C_2H_3N intermediate(s) and indirect scattering dynamics.

$$C\,(12\,amu) + ND_3\,(20\,amu) \rightarrow D_2CN\,(30\,amu) + D\,(2\,amu) \quad (1)$$

$$C_2\,(24\,amu) + NH_3\,(17\,amu) \rightarrow H_2C_2N\,(40\,amu) + H\,(1\,amu) \quad (2)$$

CM frame

We now elucidate the nature of the structural isomer(s) and the underlying reaction mechanism(s) by transforming the laboratory data (TOFs

https://doi.org/10.1038/s41550-024-02267-y

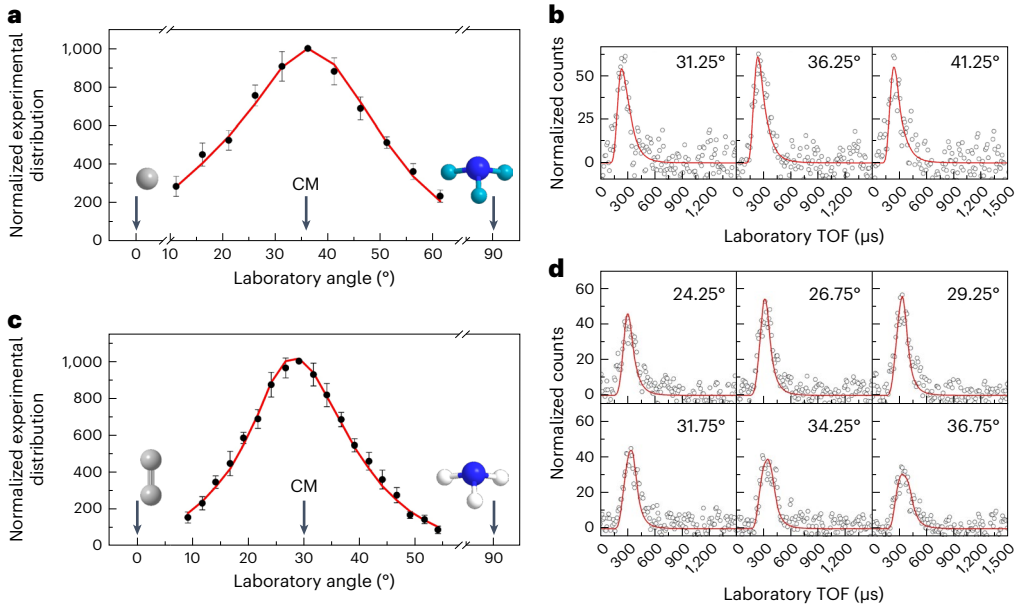

Fig. 2 | Laboratory data of the C–ND_3 and C_2–NH_3 reactions. a–d, Laboratory angular distributions (**a**,**c**) and TOFs (**b**,**d**) for the C–ND_3 (**a**,**b**) and C_2–NH_3 (**c**,**d**) reactions. The solid circles with their error bars in **a** and **c** represent the normalized experimental distribution with $\pm1\sigma$ uncertainty (s.d. of the integrals of the TOF spectra for the respective angle); the open circles indicate the experimental data. To obtain reasonable signal-to-noise ratios, for the C–ND_3 and C_2–NH_3 systems, at each angle, 3×10^6 (30 h) and 2×10^6 (20 h) TOF spectra had to be averaged, respectively. The red lines represent the best fits obtained. Atoms are colour-coded as follows: carbon, grey; nitrogen, dark blue; deuterium, light blue; hydrogen, white.

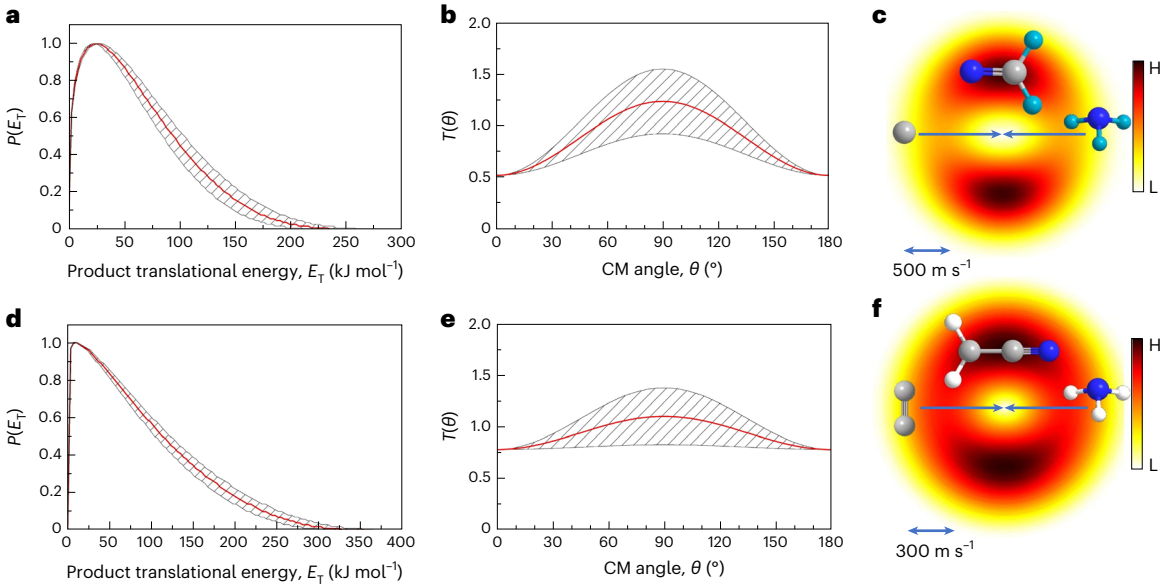

Fig. 3 | CM functions of the C–ND_3 and C_2–NH_3 reactions. a–f, CM translational energy distributions ($P(E_T)$; **a**,**d**), angular flux distributions ($T(\theta)$; **b**,**e**) and the corresponding flux contour map (**c**,**f**) for the C–ND_3 (**a**–**c**) and C_2–NH_3 (**d**–**f**) reactions. The red lines represent the best fit and shaded areas depict the error limits of the best fits. The flux contour map represents the flux intensity as a function of product velocity (u) and CM scattering angle (θ). The colour bar indicates the flux gradient from high (H) to low (L) intensity.

and LAD) into the CM reference frame[32]. This forward-convolution approach yields the CM translational energy ($P(E_T)$) and angular ($T(\theta)$) flux distributions as detailed in Fig. 3a–c, in which θ represents the CM scattering angle. For the C (^{3}P)–ND_3 (X^1A_1) system, the signal at 30 could be replicated with a single D-loss channel (reaction (1)). A detailed inspection of the $P(E_T)$ reveals a high-energy cut-off of 237 ± 25 kJ mol^{-1}, which denotes the sum of the collision energy E_c (28.1 ± 0.9 kJ mol^{-1}) plus the reaction exoergicity for molecules generated without internal excitation. Therefore, reaction (1) is suggested to be exoergic by 209 ± 26 kJ mol^{-1}. Furthermore, the $P(E_T)$ shows a distribution maximum at 26 ± 3 kJ mol^{-1}, suggesting a tight-exit transition state upon unimolecular decomposition of the D_3CN intermediate to the separated products and a substantial electron density reorganization. The $T(\theta)$ function depicts the flux across the complete angular range together with a forward–backward symmetric scattering pattern. These findings reveal indirect scattering dynamics through long-lived D_3CN complex(es) holding lifetime longer than the(ir) rotational periods[32].

Considering the C_2 ($X^1\Sigma_g^+/a^3\Pi_u$)–NH_3 (X^1A_1) system, the laboratory data can be replicated with a single atomic H-loss channel (reaction (2); Fig. 3d–f). The $P(E_T)$ as depicted in Fig. 3d shows an E_{max} of

https://doi.org/10.1038/s41550-024-02267-y

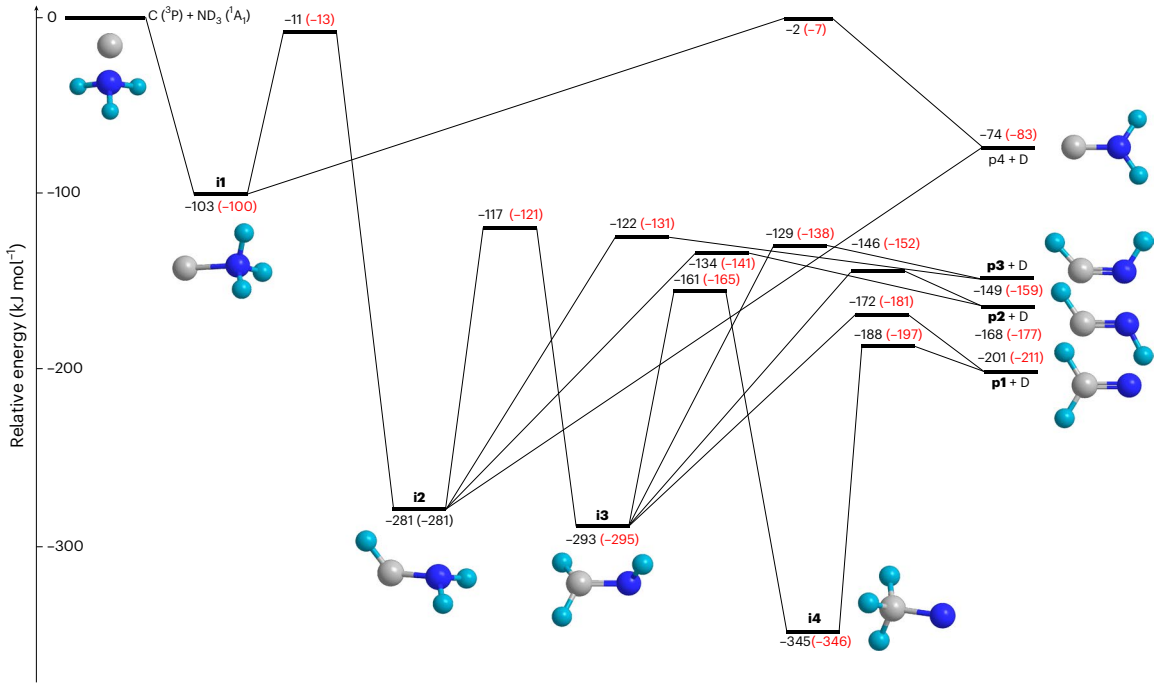

Fig. 4 | PESs of the reactions of C–ND$_3$. The energies shown in black are relative energies for the deuterated reactants and the energies in red refer to the hydrogenated reactants.

327 ± 26 kJ mol^{-1}; this results in an exoergicity of 310 ± 26 kJ mol^{-1} or 318 ± 26 kJ mol^{-1} considering an E_c of 17.0 ± 0.3 kJ mol^{-1} for dicarbon reactants in the ground $X^1\Sigma_g^+$ or excited $a^3\Pi_u$ states. It should be noted that the $P(E_T)$ peaks only slightly away from zero translational energy at 9 ± 1 kJ mol^{-1}, indicating a loose-exit transition state with only a minor rearrangement of the electron density. Finally, the $T(\theta)$ function shows a forward–backward symmetry with sideway scattering and hence a distribution maximum at 90°. These results also indicate indirect scattering dynamics[33].

Electronic structure calculations and reaction mechanisms

First, our computations on the triplet CND_3 potential energy surface (PES) reveal four reaction intermediates (**i1**–**i4**), four product channels (**p1**–**p4**) and ten transition states. These high-level calculations predict relative energies of the transition states, local minima and products within 8 kJ mol^{-1} (ref. 34,35). Four D-atom-loss pathways lead to D2-methylene amidogen (**p1**, $D_2CN\cdot$, C_{2v}, X^2B_2), *trans*-D2-iminomethyl (**p2**, DCND, C_s, X^2A'), *cis*-D2-iminomethyl (**p3**, DCND, C_s, X^2A') and D2-aminomethylidyne (**p4**, D_2NC, C_{2v}, X^2B_2). The relative energies of these isomers are within 3 kJ mol^{-1} compared with two previous studies[36,37]. A comparison of the theoretically predicted reaction energies (Fig. 4) with our experimentally derived exoergicity of 209 ± 26 kJ mol^{-1} reveals that at least the thermodynamically most stable product **p1** is formed. Contributions from high-energy isomers **p2**–**p4** might be masked in the low-energy section of the $P(E_T)$ and cannot be eliminated. The reaction is predicted to be initiated via a barrierless addition of the carbon atom to the non-bonding electron pair at the nitrogen atom of ammonia, leading to **i1** (CND_3, D3-ammoniamethylidyne) bound by 103 kJ mol^{-1}. This collision complex may eliminate a D atom, forming **p4** by passing a transition state located only 2 kJ mol^{-1} below the separated reactants, or isomerizes to **i2** ($DCND_2$, D3-aminomethylidene) via deuterium migration from nitrogen to carbon. The transition state resides 11 kJ mol^{-1} below the separated reactants and hence is preferred compared with the unimolecular decomposition of **i1** to **p4** plus D. **i2** can fragment via D loss to **p2** or **p3** through tight transition states; **p4** may be formed barrierlessly, too. Alternatively, **i2** may isomerize to **i3** (D_2CND, D3-methanimine) via a deuterium shift. This intermediate can undergo three distinct decomposition pathways through D loss leading to **p3**, **p2** and/or the thermodynamically most stable isomer **p1** involving tight-exit transition states (**i3** → **p3**, 20 kJ mol^{-1}; **i3** → **p2**, 22 kJ mol^{-1}; **i3** → **p1**, 29 kJ mol^{-1}; the numbers indicate the barrier with respect to the products). Finally, **i3** may undergo a deuterium shift to **i4** (D_3CN, D3-methylnitrene), the global minimum of the D_3CN PES, followed by unimolecular decomposition to **p1**.

Statistical Rice–Ramsperger–Kassel–Marcus calculations were also conducted to predict the branching ratios of **p1**–**p4** theoretically[34]. Within the limit of a complete energy randomization, **p1**, **p2**, **p3** and **p4** contribute 7%, 33%, 29% and 31%, respectively, at the experimental E_c of 28.1 kJ mol^{-1}. At the low-temperature conditions of TMC-1 and Titan, fractions of 8%, 41%, 33% and 18% are predicted. Under the atmospheric conditions of Titan, one peculiarity exists. A rapid suprathermal H-atom-assisted isomerization processes can efficiently convert the high-energy isomers **p3** and **p4** to **p1**[38,39]. These processes are very efficient due to absence of a barrier of **p4** + H → **i2** and a small barrier of only 20 kJ mol^{-1} for **p3** + H → **i3**. As depicted in Extended Data Fig. 1, the elevated rate constants of **p3** + H of a few 10^{-10} cm^3 s^{-1} can be reached with suprathermal H atoms possessing high kinetic energies (Supplementary Note 1).

Second, for the C_2–NH_3 system, the primary reactant beam contains dicarbon not only in its electronic ground state ($X^1\Sigma_g^+$) but also in its first electronically excited state ($a^3\Pi_u$). The calculations reveal that C_2 ($a^3\Pi_u$) does not form any bound intermediates upon collision with ammonia, but rather reacts in a direct fashion via hydrogen abstraction forming the ethynyl radical ($C_2H\cdot$, $X^2\Sigma^+$) plus the amino radical ($NH_2\cdot$, X^2B_1) in an exoergic reaction (−36 kJ mol^{-1}) through a barrier of 22 kJ mol^{-1}. However, on the singlet surface, dicarbon adds barrierlessly to the non-bonding electron pair of the nitrogen atom of ammonia to **i1′** ($CCNH_3$, ammoniaethynyl). Among the product isomers, **p1′** ($H_2CCN\cdot$; cyanomethyl; C_{2v}; $^2B_1$) represents the thermodynamically most stable isomer followed by **p2′** (H_2CNC; isocyanomethyl; C_{2v}; $^2B_1$) and **p3′** (HCCNH; imidogenacetylene; C_s; $^2A'$). The calculated relative energies of the C_2H_2N isomers agree well with previous calculations[40]. A comparison of these energies with the experimentally extracted exoergicity of 310 ± 26 kJ mol^{-1} proposed that at least **p1′** is formed under

https://doi.org/10.1038/s41550-024-02267-y

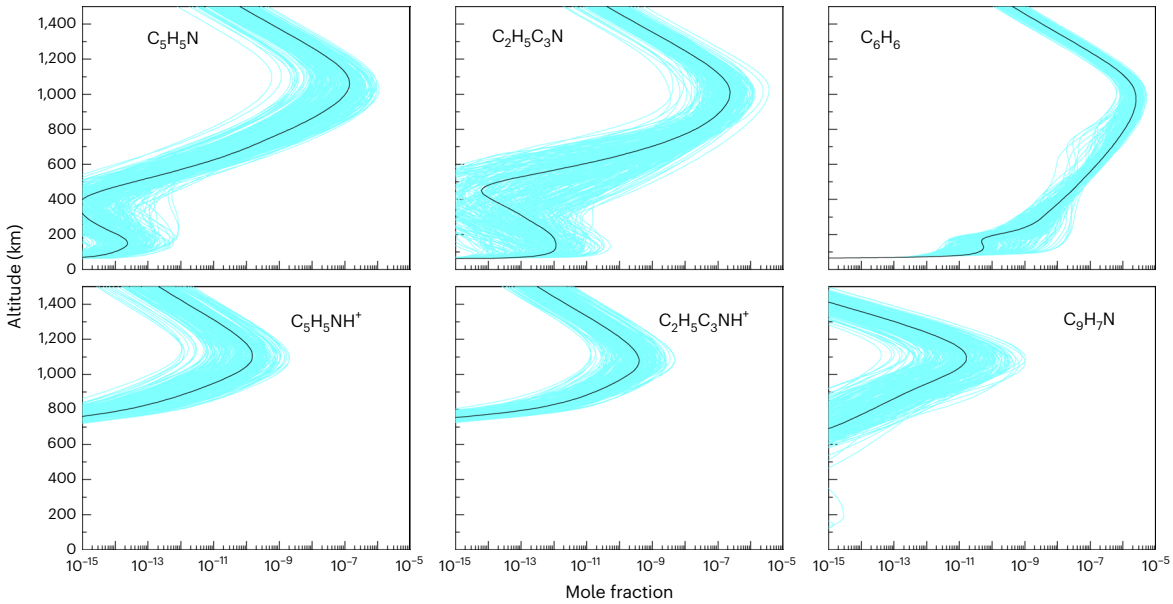

Fig. 5 | Results of the astrochemical model for Titan's atmosphere. Mole fraction profiles for six species obtained from a one-dimensional photochemical model of Titan's atmosphere. The solid black lines represent the nominal model results, with 280 runs of the Monte Carlo analysis shown as cyan lines. Please refer to the text for details on the error analysis and the assignment of the species.

single-collision conditions. Contributions from high-energy isomers **p2′**–**p5′** might be hidden in the low-energy section of the $P(E_T)$ and cannot be eliminated. **i1′** can isomerize to an exotic cyclic intermediate **i2′** ($HC(NH_2)C$) via ring closure along with a hydrogen shift from the nitrogen to the carbon or to **i4′** ($HCCNH_2$, aminoacetylene) through hydrogen migration. Our calculations also identify a loose H-loss channel to **p7′** ($CCNH_2$; aminoethynyl; C_{2v}; $^2B_1$) from **i1′**. Extensive hydrogen migration and a ring-opening pathway access intermediates **i3′** to **i9′**. The experimentally detected product **p1′** can eventually be accessed via H loss from **i6′** (H_2CCNH, aminovinyl) and/or **i7′** (CH_3CN, acetonitrile) through loose transition states. Overall, the experimentally predicted loose-exit transition state agrees well with the computational predictions of two open channels to **p1′** (H_2CCN·; cyanomethyl) via simple bond-rupture processes on the singlet surface (Extended Data Fig. 2).

From the laboratory to Titan's atmosphere

First, in Titan's atmosphere, the carbonaceous reactants (atomic carbon, dicarbon) originate from photolysis of methane (CH_4) and acetylene (C_2H_2), respectively[14,41]. Carbon can also be generated from dissociative electron–ion (CH_2^+, CH_3^+) recombination in atmospheric layers above 1,200 km (ref. 18). Ammonia abundances have been inferred indirectly via the Cassini's Ion and Neutral Mass Spectrometer (INMS) detection of the ammonium cation (NH_4^+), predicting a high mole fraction of ammonia of $(3–4) \times 10^{-5}$ at around 1,000 km (ref. 42; Supplementary Note 2). Second, the chemical reactions relevant to Titan's atmospheric chemistry must be exoergic, proceed without an entrance barrier and involve transition states with lower energy than the separated reactants. All these benchmarks are fulfilled in the formation of the H_2CN and H_2CCN radicals holding rate constants of, for example, a few 10^{-10} cm^3 s^{-1} for the C + NH_3 reaction at 50 K (ref. 43). Third, the aforementioned radicals are isoelectronic with the vinyl (C_2H_3·, X^2A') and propargyl (C_3H_3·, X^2B_1) radical. The molecular mass growth processes in Titan's atmosphere involving the H_2CN· and the H_2CCN· radicals are in strong analogy to the C_2H_3·–C_4H_3· (refs. 16,44) and C_3H_3·–C_3H_3· (ref. 45) systems, which access the phenyl radical (C_6H_5·) under single-collision conditions and benzene along with its isomers through collision with a third body. This conclusion is verified through electronic structure calculation for the H_2CN·–C_4H_3·, H_2CN·–C_4H_3· and H_2CCN·–C_3H_3· systems synthesizing three distinct pyridinyl radicals and pyridine under low-temperature conditions (Extended Data Figs. 3 and 4, and Supplementary Note 3). In the presence of a dense atmosphere such as that of Titan, pyridine can be stabilized by a third body with a bath molecule such as molecular nitrogen. Once stabilized, pyridine can be photolysed to pyridinyl radicals (*o*, *m*, *p*; C_5H_4N·; Fig. 1) followed by barrierless reactions with vinylacetylene (C_4H_4) to (iso)quinoline (C_9H_7N)[29]. Finally, previous photochemical models suggest that H_2CN· is produced via the reaction of atomic nitrogen with the methyl radical (CH_3)[46,47]. However, the reactions of atomic carbon and dicarbon with ammonia are not included due to the foregoing lack of reliable data on the C–NH_3 and C_2–NH_3 systems, whereas extensive computational and experimental data exist for the N–CH_3 system[37,48,49]. Here our results indicate the potential important role of C–NH_3 in the prebiotic chemistry of Titan.

The aforementioned findings are implemented into a one-dimensional photochemical atmospheric model of Titan to evaluate the eventual formation of pyridine (C_5H_5N) and (iso)quinoline (C_9H_7N) (Supplementary Note 2). This model incorporates an unbiased chemistry of neutrals and cations along with the coupling between them from the lower atmosphere to the ionosphere[50,51]. The chemical scheme operated in the present model has been enhanced with the new reactions studied included[51–53]. To evaluate the uncertainties of the nominal model profiles, a Monte Carlo simulation was performed according to the method described in ref. 52 (Fig. 5). These photochemical models yield exciting results. First, these studies reveal that two C_5H_5N isomers, pyridine (C_5H_5N) and ethylcyanoacetylene (C_2H_5CCCN), show notable mole fractions of 1.4×10^{-7} and 2.3×10^{-7} in the ionosphere of Titan, respectively. The maximum mole fraction for (iso)quinoline is predicted to be 1.7×10^{-11} around 1,100 km, which should be observable spectroscopically. These models also predict that the mole fraction of $(1.5 \pm 0.3) \times 10^{-9}$ at $m/z = 80$ ($C_5H_5NH^+$) derived from the Cassini INMS data[18,54] agrees well with the sum of mole fractions of $C_5H_5NH^+$ and $C_2H_5C_3NH^+$ of the atmospheric models ranging between 2.5×10^{-9} and 5.4×10^{-10}. Although the atmospheric models provide compelling constraints on the abundances of pyridine and (iso)quinoline, we have to concede that the uncertain abundances of ammonia in Titan's atmosphere, which may vary over at least two orders of magnitude, make it difficult to quantify the contributions of distinct pathways to the H_2CN· radical. With a low predicted ammonia mole fraction of a few 10^{-7}, the C–NH_3 reaction hardly competes

https://doi.org/10.1038/s41550-024-02267-y

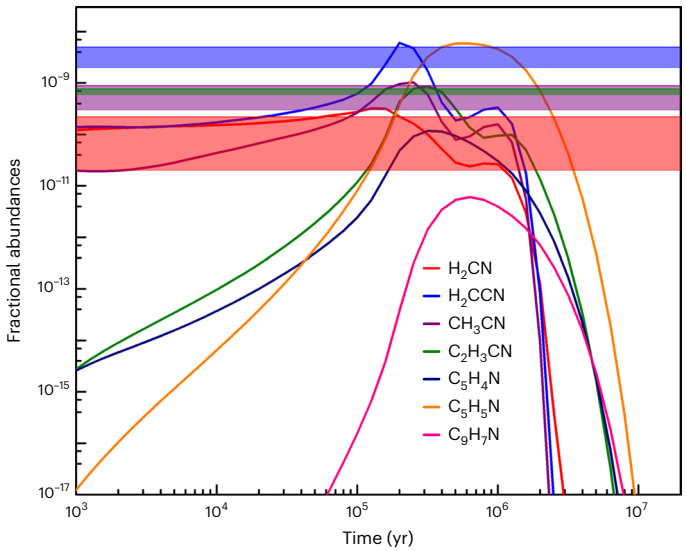

Fig. 6 | Results of the astrochemical model for TMC-1. The fractional abundance of the gas-phase methylene amidogen (H_2CN, red), cyanomethyl (H_2CCN, blue), methyl cyanide (CH_3CN, purple), vinyl cyanide (C_2H_3CN, olive), pyridinyl (C_5H_4N, navy), pyridine (C_5H_5N, orange) and (iso)quinoline (C_9H_7N, pink) are plotted as a function of time. Astronomically observed fractional abundances of the four species are visualized with the coloured horizontal bars.

with the N–CH_3 system, providing small fractions of up to 1% at most. However, considering the bimolecular nature of the C–NH_3 system, an increase of the fractional abundance of NH_3 will lead to an enhancement of H_2CN· radicals. Only future direct spectroscopic measurements of NH_3 can resolve this issue. In fact, based on the nominal model results, it can be determined that at least 10% of H_2CN· radicals are produced by the C–NH_3 reaction under conditions of high ammonia mole fraction derived from the INMS data[42]. Therefore, fundamental bimolecular reactions, including atomic carbon and dicarbon with ammonia, may initiate a chain of barrierless reactions ultimately to pyridine and (iso) quinoline. These processes are not limited to Titan, but represent versatile pathways eventually leading to NPAHs in atmospheres of planets and their moons in the outer solar systems such as on Triton[30] and Pluto[31] with organic haze layers recently detected by the New Horizons mission[55]. Only recently, the NPAH product quinolizinium$^+$ ($C_9H_8N^+$) was formed via reaction of the pyridine cation with acetylene in low-temperature pathways, highlighting the role of ion–molecule reactions in the NPAH formation in Titan's atmosphere[56]. The combined ion–molecule and neutral–neutral reaction network may finally reproduce the astronomical detected abundances of PAHs, which are drastically underestimated in current modelling[57]. Thus our understanding of fundamental low-temperature molecular mass growth processes to nitrogen-substituted aromatics and their radicals is deepened.

From the laboratory to cold molecular clouds

To explore the chemistry leading eventually to nitrogen heteroaromatics, we untangled the role of the cyanomethyl (H_2CCN·) and methylene amidogen (H_2CN·) radicals in the formation of pyridine (C_5H_5N), pyridinyl (C_5H_4N·) and (iso)quinoline (C_9H_7N) using the University of Manchester Institute of Science and Technology database (RATE2012)[58] operated with the single-point time-dependent astrochemical models[27] (Supplementary Information). The predictive capabilities of the model are verified by comparing the relevant species observed with modelled fractional abundances.

These models revealed fascinating findings (Fig. 6). First, the remarkable performance of the astrochemical model for TMC-1 can be benchmarked for the methylene amidogen radical (H_2CN·)[59], the cyanomethyl radical (H_2CCN·)[60], vinyl cyanide (C_2H_3CN)[61] and methyl cyanide (CH_3CN)[62] with astronomically observed fractional abundances of $(1.1 \pm 0.9) \times 10^{-10}$, $(3.5 \pm 1.5) \times 10^{-9}$, $(7.0 \pm 1.0) \times 10^{-10}$ and $(6.0 \pm 3.0) \times 10^{-10}$ relative to molecular hydrogen. Predicted peak abundances of H_2CN· and H_2CCN· of $(3.3 \pm 0.3) \times 10^{-10}$ at 1.3×10^5 yr and $(6.0 \pm 0.4) \times 10^{-9}$ at 2.0×10^5 yr replicate the astronomical observations nicely. Here the C–NH_3 system can account for 30% to 75% of the observed methylene amidogen radicals; generally speaking, as the initial abundances of nitrogen increase or carbon decreases, the fraction of methylene amidogen rises. Even for standard abundances of carbon versus nitrogen in TMC-1 without grain ejection, the reaction of dicarbon with ammonia contributes up to 75% to the peak abundance of the cyanomethyl radical (H_2CCN·) (Supplementary Note 4). Second, a complex chain of reactions initiated by barrierless reactions of the cyanomethyl (H_2CCN·) and methylene amidogen (H_2CN·) radicals drive molecular mass growth processes to pyridine (C_5H_5N), pyridinyl (C_5H_4N·) and (iso)quinoline (C_9H_7N) with predicted peak fractional abundances of $(6.0 \pm 0.3) \times 10^{-9}$ (6.3×10^5 yr), $(1.2 \pm 0.1) \times 10^{-10}$ (3.2×10^5 yr) and $(6.0 \pm 0.4) \times 10^{-12}$ (6.3×10^5 yr), respectively. The H_2CN·/C_4H_3· and H_2CCN·/C_3H_3· reactions produce 46% and 54% of the predicted abundances of pyridinyl (C_5H_4N·), respectively. These results suggest that at least pyridine (C_5H_5N) and pyridinyl (C_5H_4N·) might be detectable by radio telescopes such as the Green Bank Observatory and Yebes Radio Telescope in TMC-1.

Conclusion

Our studies provide persuasive evidence on the formation of the methylene amidogen radical (H_2CN·, X^2B_2) and of the resonantly stabilized cyanomethyl radical (H_2CCN·, X^2B_1) via bimolecular reactions of atomic carbon (C, ^3P) and of dicarbon (C_2, $X^1\Sigma_g^+/a^3\Pi_u$) with ammonia (NH_3, X^1A_1) in low-temperature extraterrestrial environments. Combined with modelling, these findings reveal further that both the methylene amidogen and the cyanomethyl radicals can initiate a complex chain of reactions leading to pyridine (**1**), pyridinyl radicals (**9**–**11**) and eventually to (iso)quinoline (**2**/**3**) as the simplest prototype NPAHs and potential feedstock for more complex nitrogen-based aromatics in deep space. Whereas the elementary reactions of carbon and dicarbon with ammonia can account for up to 75% of the methylene amidogen and of the cyanomethyl radical in TMC-1, their contributions in Titan's atmosphere are less constrained; this is predominantly based on the uncertain abundances of atmospheric ammonia diverging by at least two orders of magnitude. This can only be solved through future in situ observations by, for example, the prospective Dragonfly mission. However, pyridine (**1**) and (iso)quinoline (**2**/**3**)—the most primitive nitrogen aromatics—have been detected in the Murchison (CM2) carbonaceous chondrite meteorite with abundances of up to 0.5 μg g^{-1} (ppm)[63,64], thus providing a critical link between the low-temperature chemistry in cold molecular clouds and their delivery to our Solar System in the form of meteorites. Overall, the present study provides a template for a systematic investigation of elementary reactions so that a comprehensive picture of the low-temperature chemistry leading to biorelevant molecules in extraterrestrial environments emerges.

Methods

Crossed molecular beams

C–ND_3 system. The bimolecular reaction of ground-state atomic carbon (C, ^3P) with D3-ammonia (ND_3, X^1A_1) was explored under single-collision conditions using a crossed molecular beams machine (Supplementary Fig. 1)[32]. A supersonic beam of atomic carbon was produced by ablating a rotating graphite rod at 266 nm (Nd:YAG, 10–12 mJ per pulse, 30 Hz). The ablated carbon species were seeded in helium gas (99.9999%, 4 atm, 60 Hz). The primary carbon beam was velocity-selected by a chopper wheel (120 Hz) after passing through a skimmer, revealing a well-defined peak velocity v_p of 2,512 ± 49 m s^{-1} and speed ratio S of 2.9 ± 0.3 (Supplementary Table 1). Carbon atoms in the primary beam are only in the ground state (^3P) under these conditions. Operation

conditions were optimized that dicarbon in the primary beam was reduced to levels of less than 5%, which does not interfere with the scattering signal. The secondary beam of ND_3 (Sigma-Aldrich; 99% D) was released with a backing pressure of 550 torr and 60 Hz, characterized by a v_p of 1,091 ± 25 m s^{-1} and an S of 10.1 ± 1.3. Finally, the carbon beam crossed the ND_3 beam perpendicularly in the interaction region resulting in an E_c of 28.1 ± 0.9 kJ mol^{-1} and a CM angle Θ_{CM} of 35.9 ± 0.5°.

C_2–NH_3 system. A pulsed supersonic dicarbon beam (C_2 ($X^1\Sigma_g^+/a^3\Pi_u$)) was produced exploiting the same ablation source described above. Briefly, the graphite rod was ablated by focusing the 266 nm laser output at 30 Hz and energy of 8–10 mJ per pulse. The ablated species were seeded in neon (4 atm, 99.9999%). Operation conditions and delay times were optimized to maximize dicarbon concentrations in the primary beam. Laser-induced fluorescence of dicarbon revealed both a singlet ground state ($X^1\Sigma_g^+$) and the lowest-lying triplet state ($a^3\Pi_u$) along with the ro-vibrational distribution. The rotational temperature (T_{rot}) for the vibrational levels of $v = 0, 1$ of the $a^3\Pi_u$ state were measured to be 240 ± 30 K and 190 ± 30 K with fractions of 0.67 ± 0.05 and 0.33 ± 0.05, respectively, via the Swan band transition ($d^3\Pi_g$–$a^3\Pi_u$). The singlet state was detected via the Mulliken excitation ($D^1\Sigma_u^+$–$X^1\Sigma_g^+$) and the bimodal rotational distributions of both $v = 0, 1$ were revealed at fractions of 0.83 ± 0.10 and 0.17 ± 0.04, respectively. The rotational temperature of the first and second vibrational levels was derived to be 200 K with population fraction of 0.44 ± 0.05 and 0.06 ± 0.02 together with 1,000 K with fraction of 0.39 ± 0.05 and 0.11 ± 0.02, respectively[65]. The secondary ammonia (Matheson, 99.99%) beam was released with 550 torr backing pressure. The peak velocities, speed ratios of the primary and secondary beam along with the derived E_c and Θ_{CM} of the C_2–NH_3 system are tabulated in Supplementary Table 1.

For both reactions, the products were detected by a rotatable detection system under ultrahigh-vacuum conditions (6×10^{-12} torr). In detail, the neutral species were ionized with an electron impact ionizer (80 eV; 2 mA) before they were mass-selected by a quadrupole mass spectrometer in the TOF mode (Supplementary Fig. 2). The ions at a selected m/z will eventually lead to the signal detected and filtered by a photomultiplier tube (model 8850; −1.35 kV) and a discriminator (1.6 mV). Finally, a multichannel scaler is used to collect the TOF spectra at different angles. These laboratory data are converted into the CM frame with a forward-convolution method yielding the CM translational energy ($P(E_T)$) and angular ($T(\theta)$) flux distributions, with which information on the reaction dynamics can be extracted[32]. The reactive differential cross-section, $I(u, \theta) \approx P(u) \times T(\theta)$, which reports the product intensity (I) as a function of the CM angle θ and the velocity u, represents an overall image of the reaction and contains all the information of the scattering process[32].

Electronic structure calculations. The electronic structure calculations reported in this work for the carbon and dicarbon reactions with ammonia (Fig. 3, Extended Data Fig. 2 and Supplementary Data 1) were performed with the MOLPRO[66] software. The geometry optimizations and harmonic frequencies calculations used the coupled-cluster singles and doubles plus perturbative triples (CCSD(T)) method[67]. For such optimizations and frequencies, the augmented correlation consistent family basis set aug-cc-pVXZ[68] was used, with a quadruple-zeta ($X = Q$) basis being used for the C–NH_3 system, and a triple-zeta ($X = T$) for $CCNH_3$. For both systems, a final single-point energy calculation was performed at the optimized geometries with the explicitly correlated CCSD(T)-F12 method[35] with the quadruple-zeta basis set cc-pVQZ-F12[69]. Using the conventional notation, the reported energies for the C–NH_3 system are therefore CCSD(T)-F12/cc-pVQZ-F12//CCSD(T)/aug-cc-pVQZ+ZPE(CCSD(T)/aug-cc-pVQZ) and for C_2–NH_3 CCSD(T)-F12/cc-pVQZ-F12//CCSD(T)/aug-cc-pVTZ+ZPE(CCSD(T)/aug-cc-pVTZ). For the larger C_5H_5N system where the PES is accessed by the $C_3H_3 + H_2CCN$, $C_4H_3 + H_2CN$, and C_4H_3 + *cis*-HCNH reactions (Extended Data Figs. 3 and 4), geometry optimizations and harmonic frequencies calculations used the density functional B3LYP method[70,71] with the cc-pVTZ basis and single-point energies were refined at the CCSD(T)-F12/cc-pVTZ-F12 level. Thus, the reported energies for C_5H_5N species are obtained at CCSD(T)-F12/cc-pVTZ-F12//B3LYP/cc-pVTZ+ZPE(B3LYP/cc-pVTZ) using the Gaussian 16[72] and MOLPRO[66] software packages.

Data availability

All data generated in this study are available in the main text and Supplementary Information.

References

1. Pizzarello, S., Huang, Y. & Fuller, M. The carbon isotopic distribution of Murchison amino acids. *Geochim. Cosmochim. Acta* **68**, 4963–4969 (2004).
2. Smith, K. E., Callahan, M. P., Gerakines, P. A., Dworkin, J. P. & House, C. H. Investigation of pyridine carboxylic acids in CM2 carbonaceous chondrites: potential precursor molecules for ancient coenzymes. *Geochim. Cosmochim. Acta* **136**, 1–12 (2014).
3. Martins, Z. et al. Extraterrestrial nucleobases in the Murchison meteorite. *Earth Planet. Sci. Lett.* **270**, 130–136 (2008).
4. Burton, A. S., Stern, J. C., Elsila, J. E., Glavin, D. P. & Dworkin, J. P. Understanding prebiotic chemistry through the analysis of extraterrestrial amino acids and nucleobases in meteorites. *Chem. Soc. Rev.* **41**, 5459–5472 (2012).
5. Andrews, H., Candian, A. & Tielens, A. G. G. M. Hydrogenation and dehydrogenation of interstellar PAHs: spectral characteristics and H_2 formation. *Astron. Astrophys.* **595**, A23 (2016).
6. Tsuge, M., Bahou, M., Wu, Y.-J., Allamandola, L. & Lee, Y.-P. The infrared spectrum of protonated ovalene in solid *para*-hydrogen and its possible contribution to interstellar unidentified infrared emission. *Astrophys. J.* **825**, 96 (2016).
7. Tielens, A. G. G. M. Interstellar polycyclic aromatic hydrocarbon molecules. *Annu. Rev. Astron. Astrophys.* **46**, 289–337 (2008).
8. Knorke, H., Langer, J., Oomens, J. & Dopfer, O. Infrared spectra of isolated protonated polycyclic aromatic hydrocarbon molecules. *Astrophys. J.* **706**, L66 (2009).
9. Hudgins, D. M., Bauschlicher, C. W. Jr & Allamandola, L. J. Variations in the peak position of the 6.2 μm interstellar emission feature: a tracer of N in the interstellar polycyclic aromatic hydrocarbon population. *Astrophys. J.* **632**, 316 (2005).
10. Herbst, E. & Van Dishoeck, E. F. Complex organic interstellar molecules. *Annu. Rev. Astron. Astrophys.* **47**, 427–480 (2009).
11. Kaiser, R. I. & Hansen, N. An aromatic universe—a physical chemistry perspective. *J. Phys. Chem. A* **125**, 3826–3840 (2021).
12. Peeters, Z., Botta, O., Charnley, S. B., Ruiterkamp, R. & Ehrenfreund, P. The astrobiology of nucleobases. *Astrophys. J.* **593**, L129 (2003).
13. Hörst, S. M. Titan's atmosphere and climate. *J. Geophys. Res.* **122**, 432–482 (2017).
14. Vuitton, V., Yelle, R. V., Klippenstein, S. J., Hörst, S. M. & Lavvas, P. Simulating the density of organic species in the atmosphere of Titan with a coupled ion–neutral photochemical model. *Icarus* **324**, 120–197 (2019).
15. Loison, J. C. et al. The neutral photochemistry of nitriles, amines and imines in the atmosphere of Titan. *Icarus* **247**, 218–247 (2015).
16. Kislov, V. V., Nguyen, T. L., Mebel, A. M., Lin, S. H. & Smith, S. C. Photodissociation of benzene under collision-free conditions: an ab initio/Rice–Ramsperger–Kassel–Marcus study. *J. Chem. Phys.* **120**, 7008–7017 (2004).
17. Lin, M.-F. et al. Photodissociation dynamics of pyridine. *J. Chem. Phys.* **123**, 054309 (2005).
18. Vuitton, V., Yelle, R. V. & McEwan, M. J. Ion chemistry and N-containing molecules in Titan's upper atmosphere. *Icarus* **191**, 722–742 (2007).

19. Ricca, A., Bauschlicher, C. W. Jr & Bakes, E. A computational study of the mechanisms for the incorporation of a nitrogen atom into polycyclic aromatic hydrocarbons in the Titan haze. *Icarus* **154**, 516–521 (2001).
20. Soorkia, S. et al. Direct detection of pyridine formation by the reaction of CH (CD) with pyrrole: a ring expansion reaction. *Phys. Chem. Chem. Phys.* **12**, 8750–8758 (2010).
21. López-Puertas, M. et al. Large abundances of polycyclic aromatic hydrocarbons in Titan's upper atmosphere. *Astrophys. J.* **770**, 132 (2013).
22. Anderson, C. M. & Samuelson, R. E. Titan's aerosol and stratospheric ice opacities between 18 and 500 μm: vertical and spectral characteristics from Cassini CIRS. *Icarus* **212**, 762–778 (2011).
23. Sebree, J. A., Trainer, M. G., Loeffler, M. J. & Anderson, C. M. Titan aerosol analog absorption features produced from aromatics in the far infrared. *Icarus* **236**, 146–152 (2014).
24. Ali, A., Sittler, E. C. Jr, Chornay, D., Rowe, B. R. & Puzzarini, C. Organic chemistry in Titan's upper atmosphere and its astrobiological consequences: I. Views towards Cassini Plasma Spectrometer (CAPS) and Ion Neutral Mass Spectrometer (INMS) experiments in space. *Planet. Space Sci.* **109**, 46–63 (2015).
25. Mathé, C., Gautier, T., Trainer, M. G. & Carrasco, N. Detection opportunity for aromatic signature in Titan's aerosols in the 4.1–5.3 μm range. *Astrophys. J. Lett.* **861**, L25 (2018).
26. Zhao, L. et al. Gas-phase synthesis of corannulene—a molecular building block of fullerenes. *Phys. Chem. Chem. Phys.* **23**, 5740–5749 (2021).
27. Kaiser, R. I. et al. Gas-phase synthesis of racemic helicenes and their potential role in the enantiomeric enrichment of sugars and amino acids in meteorites. *Phys. Chem. Chem. Phys.* **24**, 25077–25087 (2022).
28. Parker, D. S. N. & Kaiser, R. I. On the formation of nitrogen-substituted polycyclic aromatic hydrocarbons (NPAHs) in circumstellar and interstellar environments. *Chem. Soc. Rev.* **46**, 452–463 (2017).
29. Zhao, L. et al. A molecular beam and computational study on the barrierless gas phase formation of (iso)quinoline in low temperature extraterrestrial environments. *Phys. Chem. Chem. Phys.* **23**, 18495–18505 (2021).
30. Broadfoot, A. L. et al. Ultraviolet spectrometer observations of Neptune and Triton. *Science* **246**, 1459–1466 (1989).
31. Moores, J. E., Smith, C. L., Toigo, A. D. & Guzewich, S. D. Penitentes as the origin of the bladed terrain of Tartarus Dorsa on Pluto. *Nature* **541**, 188–190 (2017).
32. Yang, Z. et al. Gas-phase formation of 1, 3, 5, 7-cyclooctatetraene (C_8H_8) through ring expansion via the aromatic 1, 3, 5-cyclooctatrien-7-yl radical ($C_8H_9^{\bullet}$) transient. *J. Am. Chem. Soc.* **144**, 22470–22478 (2022).
33. Yang, Z. et al. Gas-phase formation of the resonantly stabilized 1-indenyl ($C_9H_7^{\bullet}$) radical in the interstellar medium. *Sci. Adv.* **9**, eadi5060 (2023).
34. Zhang, J. & Valeev, E. F. Prediction of reaction barriers and thermochemical properties with explicitly correlated coupled-cluster methods: a basis set assessment. *J. Chem. Theory Comput.* **8**, 3175–3186 (2012).
35. Adler, T. B., Knizia, G. & Werner, H.-J. A simple and efficient CCSD(T)-F12 approximation. *J. Chem. Phys.* **127**, 221106 (2007).
36. Bourgalais, J. et al. The $C(^3P) + NH_3$ reaction in interstellar chemistry. I. Investigation of the product formation channels. *Astrophys. J.* **812**, 106 (2015).
37. Chiba, S., Honda, T., Kondo, M. & Takayanagi, T. Direct dynamics study of the $N(^4S)+ CH_3(^2A_2'')$ reaction. *Comput. Theor. Chem.* **1061**, 46–51 (2015).
38. Mebel, A. M., Georgievskii, Y., Jasper, A. W. & Klippenstein, S. J. Pressure-dependent rate constants for PAH growth: formation of indene and its conversion to naphthalene. *Faraday Discuss.* **195**, 637–670 (2016).
39. Jasper, A. W. & Hansen, N. Hydrogen-assisted isomerizations of fulvene to benzene and of larger cyclic aromatic hydrocarbons. *Proc. Combust. Inst.* **34**, 279–287 (2013).
40. Lau, K.-C., Li, W.-K., Ng, C. Y. & Chiu, S.-W. A Gaussian-2 study of isomeric C_2H_2N and $C_2H_2N^+$. *J. Phys. Chem. A* **103**, 3330–3335 (1999).
41. Willacy, K., Allen, M. & Yung, Y. A new astrobiological model of the atmosphere of Titan. *Astrophys. J.* **829**, 79 (2016).
42. Cui, J. et al. Analysis of Titan's neutral upper atmosphere from Cassini Ion Neutral Mass Spectrometer measurements. *Icarus* **200**, 581–615 (2009).
43. Hickson, K. M. et al. The $C(^3P) + NH_3$ reaction in interstellar chemistry. II. Low temperature rate constants and modeling of NH, NH_2, and NH_3 abundances in dense interstellar clouds. *Astrophys. J.* **812**, 107 (2015).
44. Pope, C. J. & Miller, J. A. Exploring old and new benzene formation pathways in low-pressure premixed flames of aliphatic fuels. *Proc. Combust. Inst.* **28**, 1519–1527 (2000).
45. Zhao, L. et al. Gas-phase synthesis of benzene via the propargyl radical self-reaction. *Sci. Adv.* **7**, eabf0360 (2021).
46. Pearce, B. K. D., Ayers, P. W. & Pudritz, R. E. A consistent reduced network for HCN chemistry in early earth and Titan atmospheres: quantum calculations of reaction rate coefficients. *J. Phys. Chem. A* **123**, 1861–1873 (2019).
47. Pearce, B. K. D., He, C. & Hörst, S. M. An experimental and theoretical investigation of HCN production in the Hadean Earth atmosphere. *ACS Earth Space Chem.* **6**, 2385–2399 (2022).
48. Marston, G., Nesbitt, F. L., Nava, D. F., Payne, W. A. & Stief, L. J. Temperature dependence of the reaction of nitrogen atoms with methyl radicals. *J. Phys. Chem.* **93**, 5769–5774 (1989).
49. Marston, G., Nesbitt, F. L. & Stief, L. J. Branching ratios in the $N + CH_3$ reaction: formation of the methylene amidogen (H_2CN) radical. *J. Chem. Phys.* **91**, 3483–3491 (1989).
50. Dobrijevic, M., Loison, J. C., Hickson, K. M. & Gronoff, G. 1D-coupled photochemical model of neutrals, cations and anions in the atmosphere of Titan. *Icarus* **268**, 313–339 (2016).
51. Loison, J. C., Dobrijevic, M. & Hickson, K. M. The photochemical production of aromatics in the atmosphere of Titan. *Icarus* **329**, 55–71 (2019).
52. Benne, B., Dobrijevic, M., Cavalié, T., Loison, J.-C. & Hickson, K. M. A photochemical model of Triton's atmosphere with an uncertainty propagation study. *Astron. Astrophys.* **667**, A169 (2022).
53. Vanuzzo, G. et al. Reaction $N(^2D) + CH_2CCH_2$ (allene): an experimental and theoretical investigation and implications for the photochemical models of Titan. *ACS Earth Space Chem.* **6**, 2305–2321 (2022).
54. Teolis, B. D. et al. A revised sensitivity model for Cassini INMS: Results at Titan. *Space Sci. Rev.* **190**, 47–84 (2015).
55. Gladstone, G. R. & Young, L. A. New Horizons observations of the atmosphere of Pluto. *Annu. Rev. Earth Planet. Sci.* **47**, 119–140 (2019).
56. Rap, D. B., Schrauwen, J. G., Marimuthu, A. N., Redlich, B. & Brünken, S. Low-temperature nitrogen-bearing polycyclic aromatic hydrocarbon formation routes validated by infrared spectroscopy. *Nat. Astron.* **6**, 1059–1067 (2022).
57. McGuire, B. A. et al. Detection of two interstellar polycyclic aromatic hydrocarbons via spectral matched filtering. *Science* **371**, 1265–1269 (2021).
58. McElroy, D. et al. The UMIST database for astrochemistry 2012. *Astron. Astrophys.* **550**, A36 (2013).

59. Ohishi, M., McGonagle, D., Irvine, W. M., Yamamoto, S. & Saito, S. Detection of a new interstellar molecule, H_2CN. *Astrophys. J.* **427**, L51–L54 (1994).
60. Thaddeus, P., Vrtilek, J. M. & Gottlieb, C. A. Laboratory and astronomical identification of cyclopropenylidene, C_3H_2. *Astrophys. J.* **299**, L63–L66 (1985).
61. Cernicharo, J. et al. Discovery of CH_2CHCCH and detection of HCCN, HC_4N, CH_3CH_2CN, and, tentatively, CH_3CH_2CCH in TMC-1. *Astron. Astrophys.* **647**, L2 (2021).
62. Tennis, J. D. et al. Detection and modelling of CH_3NC in TMC-1. *Mon. Not. R. Astron. Soc.* **525**, 2154–2171 (2023).
63. Stoks, P. G. & Schwartz, A. W. Basic nitrogen-heterocyclic compounds in the Murchison meteorite. *Geochim. Cosmochim. Acta* **46**, 309–315 (1982).
64. Sephton, M. A. Organic compounds in carbonaceous meteorites. *Nat. Prod. Rep.* **19**, 292–311 (2002).
65. Dangi, B. B., Maity, S., Kaiser, R. I. & Mebel, A. M. A combined crossed beam and ab initio investigation of the gas phase reaction of dicarbon molecules (C_2; $X^1\Sigma_g^+/a^3\Pi_u$) with propene (C_3H_6; X^1A'): identification of the resonantly stabilized free radicals 1-and 3-vinylpropargyl. *J. Phys. Chem. A* **117**, 11783–11793 (2013).
66. Werner, H. et al. MOLPRO, version 2015.1, a package of ab initio programs (Univ. Cardiff Chemistry Consultants (UC3), 2015).
67. Knowles, P. J., Hampel, C. & Werner, H. J. Coupled cluster theory for high spin, open shell reference wave functions. *J. Chem. Phys.* **99**, 5219–5227 (1993).
68. Dunning, T. H. Jr Gaussian basis sets for use in correlated molecular calculations. I. The atoms boron through neon and hydrogen. *J. Chem. Phys.* **90**, 1007–1023 (1989).
69. Peterson, K. A., Adler, T. B. & Werner, H.-J. Systematically convergent basis sets for explicitly correlated wavefunctions: the atoms H, He, B–Ne, and Al–Ar. *J. Chem. Phys.* **128**, 084102 (2008).
70. Becke, A. D. Density-functional thermochemistry. III. The role of exact exchange. *J. Chem. Phys.* **98**, 5648–5652 (1993).
71. Lee, C., Yang, W. & Parr, R. G. Development of the Colle–Salvetti correlation-energy formula into a functional of the electron density. *Phys. Rev. B* **37**, 785 (1988).
72. Frisch, M. J. et al. Gaussian 16, revision C.1 (Gaussian Inc., Wallingford CT, 2016).

Acknowledgements

This work was supported by the US Department of Energy, Basic Energy Sciences, by grant no. DE-FG02-03ER15411 to the University of Hawaii at Manoa. The support of Conselho Nacional de Desenvolvimento Científico e Tecnológico (CNPq), grant nos. 311508/2021-9 and 405524/2021-8, is also acknowledged. We acknowledge fruitful discussions on the fractional abundances of ammonia with C. A. Nixon (NASA Goddard) and K. Willacy (JPL).

Author contributions

R.I.K. designed the experiments. Z.Y., C.H. and S.J.G. preformed the experiments. A.M.M., P.F.G.V., M.O.A. and B.R.L.G. conducted the electronic structure calculations. J.-C.L, K.M.H. and M.D. conducted the atmospheric modelling of Titan. X.L. performed the astrochemical modelling of TMC-1. Z.Y. and R.I.K. analysed the data and wrote the paper. All authors discussed the data.

Competing interests

The authors declare no competing interests.

Additional information

Extended data is available for this paper at https://doi.org/10.1038/s41550-024-02267-y.

Supplementary information The online version contains supplementary material available at https://doi.org/10.1038/s41550-024-02267-y.

Correspondence and requests for materials should be addressed to Alexander M. Mebel, Breno R. L. Galvão, Jean-Christophe Loison, Xiaohu Li or Ralf I. Kaiser.

Peer review information *Nature Astronomy* thanks Ben Pearce and Gianmarco Vanuzzo for their contribution to the peer review of this work.

https://doi.org/10.1038/s41550-024-02267-y

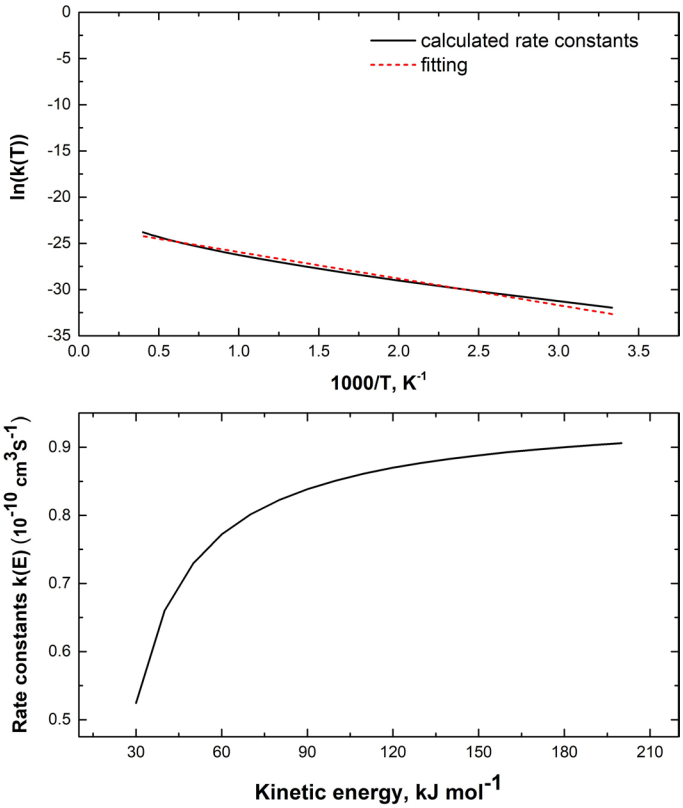

Extended Data Fig. 1 | Temperature and energy dependence of the thermal rate constants. Temperature and energy dependence of the thermal rate constant k(T) and k(E) for the **p3** + H in the C + NH_3 reaction. TST methods are utilized in the calculation.

https://doi.org/10.1038/s41550-024-02267-y

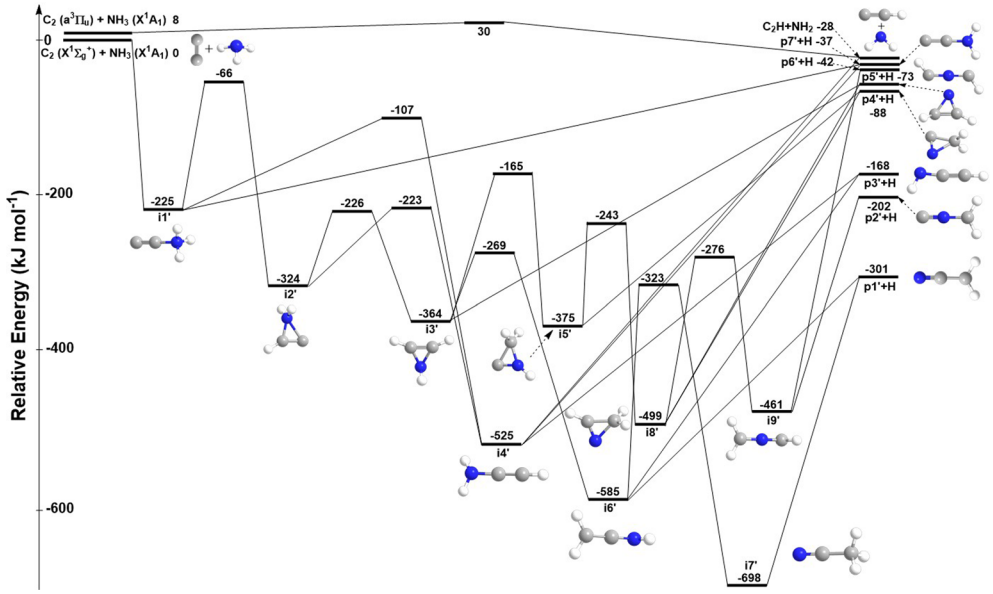

Extended Data Fig. 2 | Potential energy surfaces of the reaction of dicarbon -ammonia. Singlet and triplet surfaces of the C_2-NH_3 system involving different routes to the final products.

https://doi.org/10.1038/s41550-024-02267-y

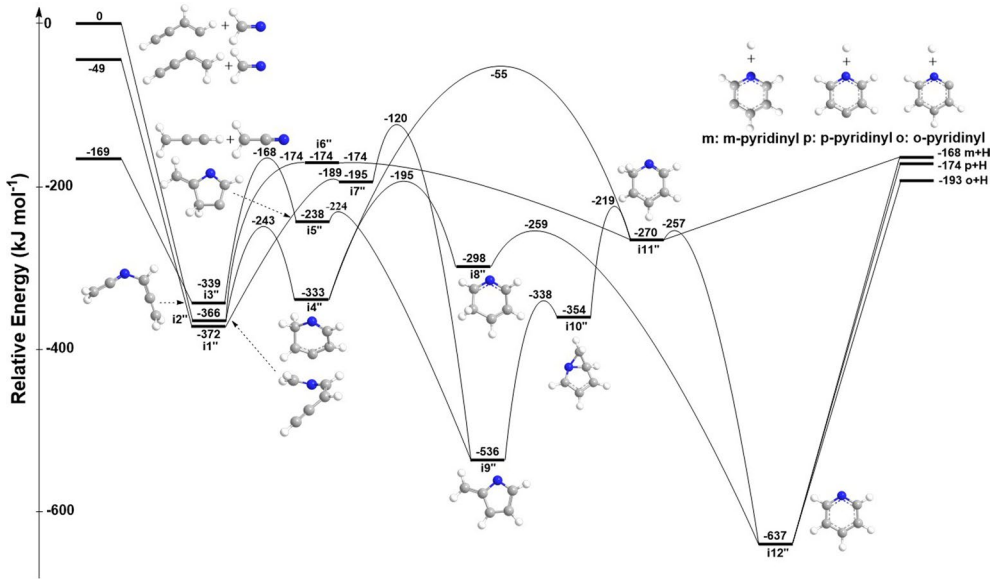

Extended Data Fig. 3 | Formation pathways to pyridinyl radicals and the pyridine intermediate I. Distinct pyridinyl radicals and pyridine can be formed from reactions of methylene amidogen (H_2CN) with *i*/*n*-C_4H_3 isomers and the cyanomethyl (H_2CCN) with propargyl (C_3H_3).

https://doi.org/10.1038/s41550-024-02267-y

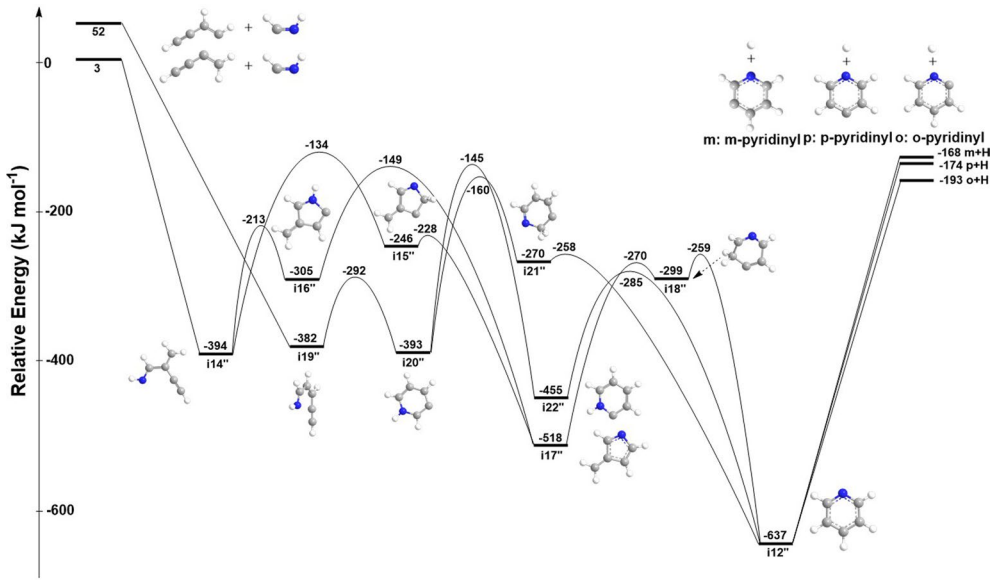

Extended Data Fig. 4 | Formation pathways to pyridinyl radicals and the pyridine intermediate II. Distinct pyridinyl radicals and pyridine can be formed from reactions of cis-iminomethyl (HCNH) with *i*/*n*-C_4H_3 isomers.